16TH EUROPEAN CONFERENCE ON EARTHQUAKE ENGINEERING THESSALONIKI 18 - 21 JUNE 2018

IMPROVING THE COLLAPSE RISK OF STEEL STRUCTURES WITH HIGH-PERFORMANCE STEEL

Yusuke SUZUKI[1], Dimitrios LIGNOS[2]

ABSTRACT

With the advent of material science, high-performance steel materials have been developed for seismic applications that potentially reduce the earthquake-induced collapse risk of steel frame buildings. The High Yield Point (HYP400) steel is one of those materials that is developed based on thermomechanical control process. Both its yield strength and notch toughness is enhanced compared to conventional seismic-resistant steels. This is achieved through refinement of the microstructural grain size. The application of such material in steel columns facilitates economic design and enhances the collapse capacity of steel moment resisting frames during severe seismic events.

This paper first discusses the key aspects of the HYP400 steel and illustrates its potential through detailed nonlinear analyses and earthquake-induced collapse simulations of a steel frame building. The material cyclic hardening prior to the onset of local buckling is characterized on the basis of uniaxial cyclic coupon tests. Finite element studies are then conducted to investigate the pre- and post-buckling behavior of hollow structural section steel columns made of HYP400 steel under various loading histories. A versatile fiber-based deterioration model is then utilized that captures the steel material potential and facilitates computationally efficient collapse simulations. The effectiveness of the HYP400 steel for enhancing the collapse capacity of a steel moment resisting frame is demonstrated through incremental dynamic analysis of a case study steel moment-resisting frame.

Keywords: High Yield Point Steel, Steel columns, Thermomechanical control process, Deterioration modeling, Collapse assessment

1. INTRODUCTION

In today's steel construction, buildings are characterized by progressively increasing height and large spans. Steel columns in a moment resisting frame (MRF) are expected to remain elastic during an earthquake event due to capacity design considerations. Therefore, stocky wide flange or Hollow Structural Section (HSS) steel columns are often used to achieve such objectives. High strength steel could be a possible solution for controlling the total weight of the steel construction. At the same time, the seismic performance of steel MRFs can be potentially improved (e.g. Wada 2008). For conventional high strength steel materials, the tradeoff is how to control the strength versus the notch toughness and weldability. Interestingly, High Yield Point (HYP400) steel has been recently developed that satisfies all the above objectives (Suzuki et. al. 2008). When it is utilized in steel columns, the strong-column-weak-beam (SCWB) ratio is enhanced because of the yield strength increase. Therefore, it is anticipated that the collapse capacity of steel MRFs designed with such columns should also increase (Elkady and Lignos 2014). However, the post-buckling behavior of steel columns that utilize HYP400 steel should be characterized such that the collapse resistance of steel MRFs can be quantified within the Performance-Based Earthquake Engineering framework (Cornell and Krawinkler 2000). Another compelling issue is the material hardening quantification. This affects

[1] Senior Researcher, Nippon Steel and Sumitomo Metal Corporation, Futtsu City, Japan, suzuki.s2k.yusuke@jp.nssmc.com

[2]Associate Professor, Swiss Federal Institute of Technology, Lausanne (EPFL), Lausanne, Switzerland, dimitrios.lignos@epfl.ch

the force redistributions within a steel MRF when steel columns experience flexural yielding. This is an important issue particularly for first story steel columns that are expected to yield at their base.

This paper first provides an overview of the key material characteristics of HYP400 steel. This is achieved through uniaxial cyclic coupon tests that facilitate the quantification of combined isotropic/kinematic hardening of HYP400 steel. The collapse behavior of HYP400 steel HSS columns is then evaluated with emphasis at large deformations through detailed finite element (FE) analyses. A versatile fiber-based deterioration model is then informed to simulate the collapse behavior of HSS steel columns within a frame analysis nonlinear finite element program. The potential of high performance steel in mitigating earthquake-induced collapse is demonstrated through collapse simulations of an 8-story steel MRF.

2. HIGH YIELD POINT STEEL

2.1 Concept of High Yield Point steel

High Yield Point steel is developed with the performance objective to maintain steel columns essentially elastic during severe seismic events such that earthquake-induced collapse and residual deformations can be controlled (Suzuki et. al. 2008). In brief, the yield strength of HYP400 steel is enhanced by utilizing thermo-mechanical controlled process (TMCP) technology (e.g., Nishioka and Ichikawa 2012). This technology provides high strength and high notch toughness through microstructural grain size refinement. Weldability can also be ensured by lowering the content of carbon and other alloying elements.

Table 1 compares major material specifications of the HYP400 steel and a conventional seismic resistant steel for steel HSS in Japan (i.e., BCP325 steel). The nominal yield strength of HYP400 steel is 400MPa, which is 23% higher compared to BCP325 steel. The nominal tensile strength of both steels is the same. Therefore, the yield-to-tensile strength ratio (YR) of HYP400 steel is raised up to 0.9 compared to the limitation of 0.8 for BCP325 steel. Increasing the tensile strength to keep the YR low results into the addition of carbon and other alloying elements that compromises weldability (i.e., carbon equivalent, C_{eq}) and notch toughness (i.e., charpy v-notch value, CVN). These are essential aspects for seismic applications such that brittle fractures can be prevented during inelastic deformations. Therefore, the tensile strength and YR limitation of HYP400 steel is also determined to ensure a minimum CVN and C_{eq} quality.

Table 1. Mechanical specifications of HYP400 and BCP325 steel

Steel	Yield strength (MPa)	Tensile strength (MPa)	Yield-to-tensile strength ratio	CVN @ 0° C (J)	C_{eq}*
HYP400	400 to 550	490 to 640	≤ 0.9	70 ≤	≤ 0.40
BCP325	325 to 445	490 to 610	≤ 0.8	27 ≤	≤ 0.44

$$* C_{eq} = C + \frac{Si}{24} + \frac{Mn}{6} + \frac{Ni}{40} + \frac{Cr}{5} + \frac{Mo}{4} + \frac{V}{14}$$

2.2 Uniaxial coupon tests

In order to characterize the material hardening of steel materials for seismic applications, representative uniaxial cyclic coupon tests should be conducted as discussed in Lignos and Suzuki (2013) and Sousa and Lignos (2017). For this purpose, uniaxial coupon tests of an HYP400 steel is conducted and compared with those of conventional BCP325 steel. Rectangular and circular coupons are extracted from different locations of HSS columns made of HYP400 and BCP325 steels. These coupons are subjected to uniaxial monotonic and cyclic load such that the material isotropic/kinematic strain hardening can be fully characterized. Referring to Figure 1a, a comparison of the monotonic tensile true stress-strain curves of the above mentioned steel materials is shown. The stress-strain curves are depicted up to uniform elongation (i.e., elongation at ultimate tensile strength). The yield

strength of the HYP400 steel is about 75MPa higher than that of BCP325 steel. After yielding, HYP400 steel does not harden as much as BCP325 steel. It is evident that the ultimate strength of the both materials is nearly the same. This is consistent with the steel specification shown previously in Table 1. The yield strength of the corner section is about 100MPa higher compared to that of the flat section in both steels. This is due to pre-straining during the manufacturing process of HSS cross-sections. Referring to Figure 1b, a comparison of the true stress-strain relations of round coupons subjected to uniaxial cyclic loading is shown. From this figure, the differential yield strength between HYP400 and BCP325 steel is inherited under cyclic loading. While the plastic strain amplitude increases, the stress difference becomes smaller, which reflect the monotonic tensile testing results (see Figure 1a).

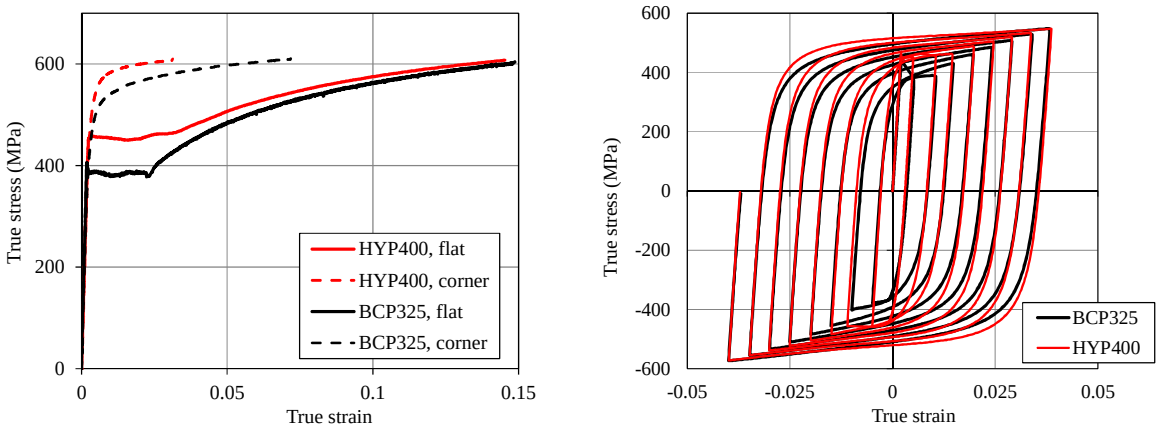

(a) monotonic tensile testing (b) uniaxial cyclic loading

Figure 1. True stress-strain relation of HYP400 and BCP325 steels

2.3 Modeling of strain hardening characteristics

The stress-strain constitutive relation of a steel material can be well represented by a nonlinear kinematic and isotropic hardening model proposed by Lemaitre and Chaboche (1975). The kinematic and isotropic hardening components are given by the following equations by assuming one backstress,

$$\dot{\alpha} = C\frac{1}{\sigma^o}(\sigma - \alpha)\dot{\varepsilon}_{pl} - \gamma\alpha\dot{\varepsilon}_{pl} \tag{1}$$

$$\sigma^o = \sigma^o\big|_0 + Q_\infty\left(1 - e^{-b\varepsilon_{pl}}\right) \tag{2}$$

in which, C is the initial kinematic hardening modulus; γ is the parameter, which determines the rate at which C decreases while plastic deformation, ε_{pl}, increases; α is the backstress; Q is the maximum change in the size of the yield surface. The parameter b defines the rate at which the size of the yield surface changes as ε_{pl} develops. These parameters can be calibrated as discussed in Sousa and Lignos (2017). Few key observations are as follows: the corner section does not exhibit isotropic hardening due to pre-straining during the manufacturing process; therefore, only C and γ may be quantified in this case. The kinematic/isotropic hardening parameters for HYP400 and BCP325 steels are identified based on a number of uniaxial coupon tests similar to the one shown in the previous section. A comparison of the predicted stress-strain relations is shown in Figure 2. In this figure, the yield strength of the flat section is assumed to be the nominal yield strength of the respective material. The yield strength of the corner section is assumed to be 100MPa higher than that of the flat section. This is consistent with observations from monotonic tensile coupon tests (see Figure 1a). Referring to Figure 2, the predicted stress strain relations reflect well the cyclic hardening characteristics of HYP400 and BCP325 steels.

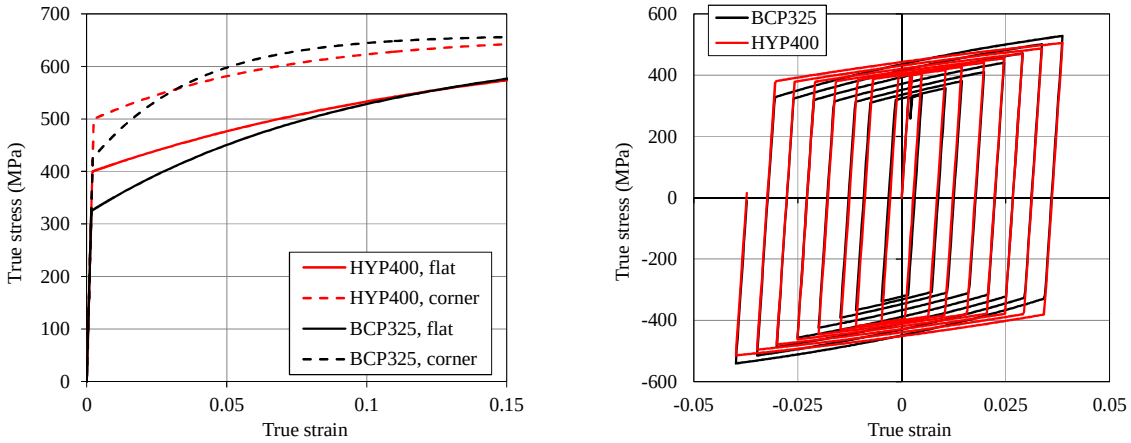

(a) monotonic tensile load (b) uniaxial cyclic load

Figure 2. Predicted stress-strain relations of HYP400 and BCP325 steel materials

3. STEEL BEAM-COLUMN FINITE ELEMENT STUDIES

3.1 FE model

In order to simulate the pre- and post-buckling behavior of HYP400 and BCP325 steel HSS columns, detailed FE analyses of HSS beam-columns are carried out. Figure 3 provides an overview of the FE model employed in this study. The FE model is developed in the FE package ABAQUS (2014). The HSS member is modeled with shell elements (S4R). The HSS column base is fully fixed. Combined lateral and axial load demands are applied on top of the HSS section. The out-of-plane deformations are constrained at the loading point. Referring to Figure 3a, residual stress distributions are considered as proposed by Kawashima et. al. (1973). In order to trigger local geometric instabilities in the FE analysis, (i.e., local buckling), a geometric imperfection proportional to the first eigen mode is introduced. The imperfection is scaled such that the maximum out-of-plane displacement Δ of the local buckling is 0.6% of the HSS depth excluding the corner section.

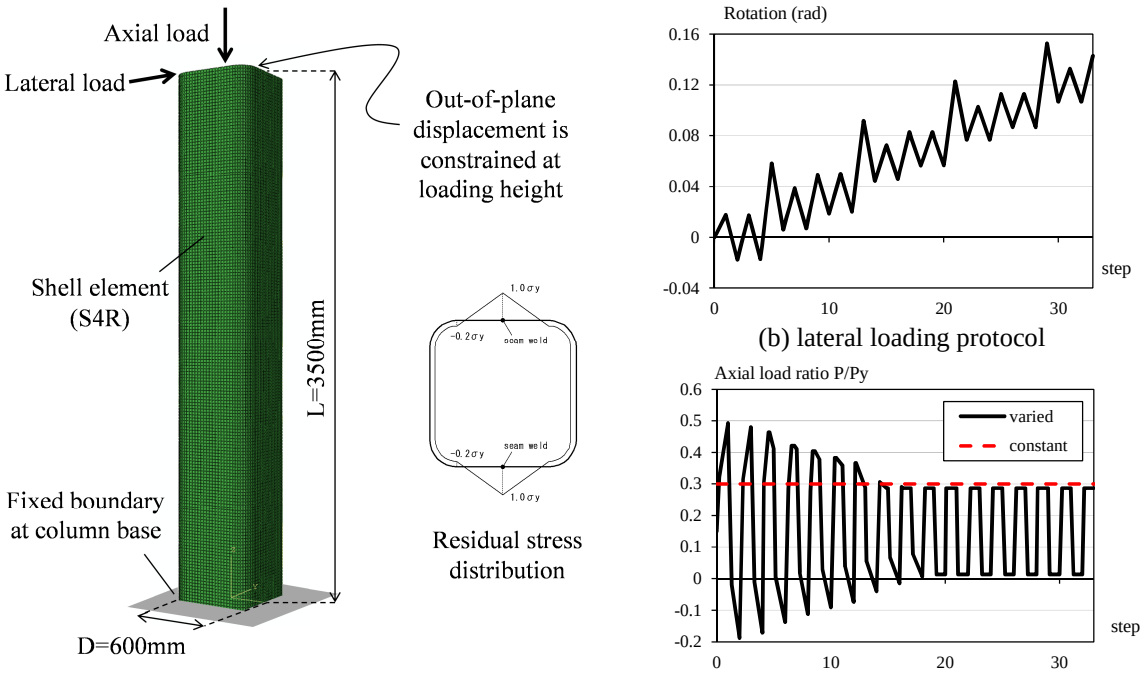

(a) modeling overview (b) lateral loading protocol (c) axial loading protocol for BCP325 columns

Figure 3. Overview of FE model and imposed loading protocols

The analyzed steel column utilizes an HSS600x22 cross-section. The corresponding HSS depth-to-thickness (D/t) ratio is 27. The shear span ratio (L/D ratio) of the analyzed model is 5.8; therefore, the corresponding loading height is 3500mm. The HYP400 and BCP325 stress-strain constitutive relations are utilized in the FE model to trace the spread of plasticity within the FE cross-section (see Figure 2). The column section geometry is the same in both cases. The FE model is subjected to: monotonic lateral load combined with constant axial load; a collapse-consistent loading protocol combined with constant and varying axial load (Suzuki and Lignos 2014) shown in Figures 3b and 3c. The loading conditions of typical interior and end steel MRF columns are properly represented in the collapse-consistent loading protocols. The axial load ratio on BCP325 steel columns for the constant axial loading protocol is 0.3. The varying axial loading protocol imposed to BCP325 steel columns has an initial gravity-induced offset of 0.15 and the applied axial load amplitude varies from 0.5 in compression to -0.2 in tension to appropriately trace dynamic overturning effects that an end steel MRF column may experience. For HYP400 steel columns, the same absolute axial load with the BCP325 steel column is applied, i.e., the imposed constant axial load ratio is 0.24; varying axial load fluctuates from 0.41 to -0.16. This is on the basis of the assumption that columns as part of a steel MRF are replaced from BCP325 steel to HYP400 steel without changing cross-section sizes.

3.2 FE results- monotonic lateral load

Figure 4 shows the moment and axial shortening versus chord rotation subjected to monotonic lateral loading. Referring to Figure 4a, the moment deteriorates due to the local buckling progression. The yield moment of the HYP400 steel column is enhanced due to the higher yield strength compared to that of the BCP325 steel column. The capping moment of the HYP400 steel column is also higher than that of the BCP325 steel column. This is attributed to the differential stress between HYP400 and BCP325 steels at relatively small plastic strain amplitudes prior to reaching the ultimate strength (see Figure 1a). The post-peak deterioration slope is initially steep. However, it gradually becomes smoother due to stabilization of the local buckling wave (Krawinkler and Zohrei 1983). The initial post-peak deterioration slope of the HYP400 steel column is steeper than that of the BCP325 steel column. After local buckling stabilization, the residual strength becomes approximately the same. Referring to Figure 4b, the progression of axial shortening is accelerated from the onset of local buckling. The extent of axial shortening of HYP400 and BCP325 steel columns is nearly the same.

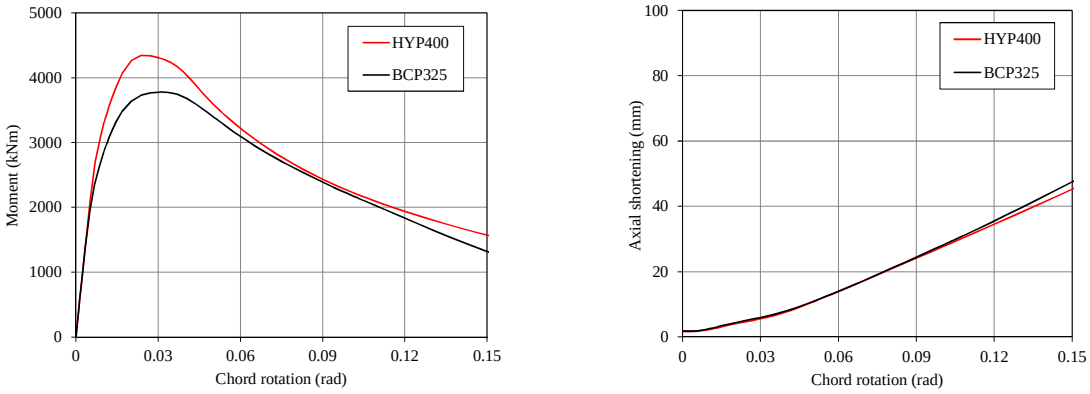

(a) moment-rotation (b) axial shortening-rotation

Figure 4. FE simulation results for monotonic lateral loading

3.3 FE results- collapse-consistent loading protocols

Figure 5 shows comparisons of the hysteretic response of HYP400 and BCP325 columns subjected to collapse-consistent loading protocols in an effort to further understand the behavior of such columns under asymmetric lateral loading (i.e., ratcheting). Referring to Figures 5a and 5b, the moment under constant axial load caps due to local buckling and it deteriorates cyclically in both loading directions. Column axial shortening grows during the imposed loading history. This is because the buckling wave is developed on both flanges and damage is accumulated during the loading cycles (see Figure 5e).

Referring to Figures 5c and 5d, the capping moment under varying axial load is reduced due to axial load variation in the compressive loading direction. In the post-capping region, the moment does not deteriorate in the tensile loading direction. As a result, residual strength at large deformations under varying axial load is higher than that of constant axial load. As such, the column axial shortening at large deformations is four times smaller compared to the column under constant axial load. The observed difference of damage accumulation is because the out-of-plane distortion of the HSS member due to local buckling is stretched back during a tensile loading excursion when lateral loading is coupled with varying axial load (see Figure 5f). These observations are consistent with prior experimental studies conducted by the authors (Suzuki and Lignos 2015 and 2017). Similar to the monotonic FE results, the main difference between the hysteretic behavior of HYP400 and BCP325 steel columns appears near the capping moment. The extent of axial shortening of these columns with respect to chord rotation is also similar.

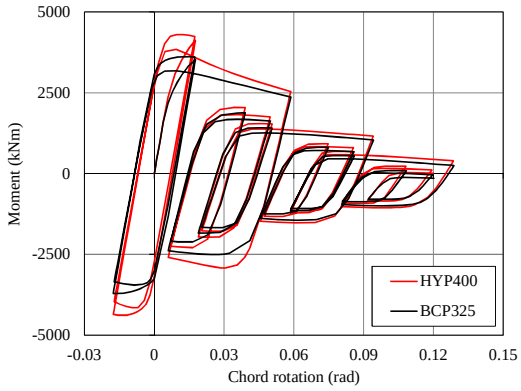

(a) moment-rotation, const. axial load

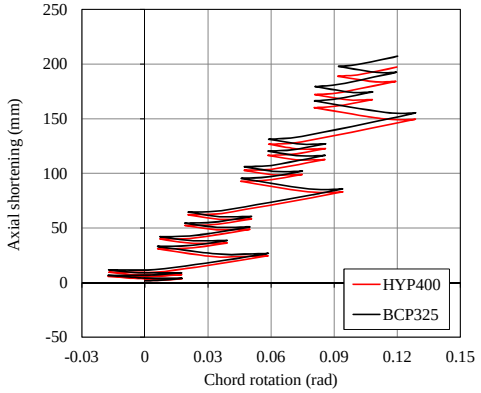

(b) axial shortening-rotation, const. axial load

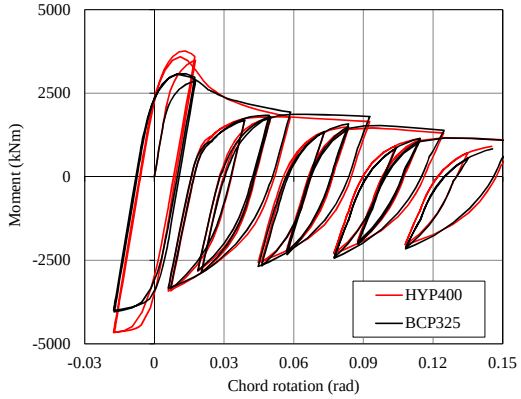

(c) moment-rotation, var. axial load

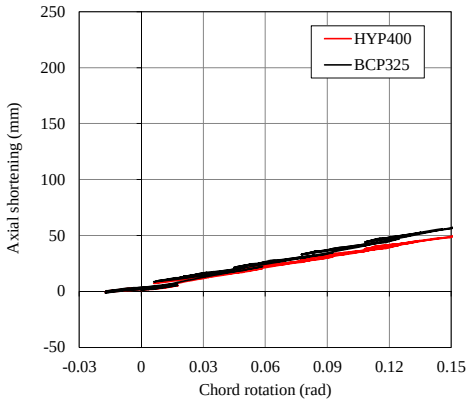

(d) axial shortening-rotation, var. axial load

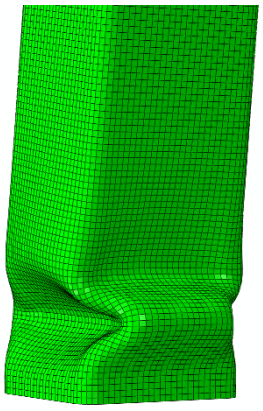

(e) HYP400 column under const. axial load at 0.12 rad.

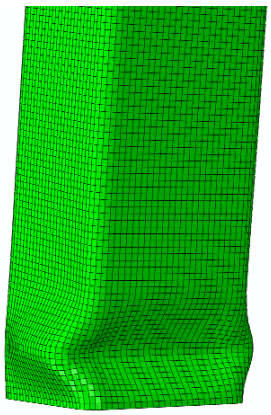

(f) HYP400 column under var. axial load at 0.12 rad.

Figure 5. Steel beam-columns subjected to collapse-consistent loading protocols

4. FIBER-BASED DETERIORATION MODEL

To assess the influence of the respective material on the overall structural behavior of steel MRFs, the observed hysteretic behavior of HYP400 and BCP325 steel columns is represented in a fiber-based deterioration model. Figure 6 shows the fiber modeling approach concept developed for steel HSS columns (Suzuki and Lignos 2017). In brief, the developed model is able to capture the axial load-flexural strength interaction and growth of axial shortening as well as strength and stiffness deterioration due to local buckling. For this purpose, a plastic hinge length equivalent to the buckling length of the column is defined at the column end, which is set to 0.8D (D is the HSS column depth) based on prior research (Suzuki and Lignos 2015 and 2017, Yamada et. al. 1993). A fiber section is assigned to this length. The fiber section can contract/elongate depending on the axial and flexural force demands that shift the neutral axis of the respective cross section as shown schematically in Figure 6b. A stress-strain constitutive relation is assigned to the fiber cross-section. This formulation captures the material strain hardening in the pre-buckling state and the column's strength deterioration in the post-buckling state. The details are summarized in prior work by the authors (Suzuki and Lignos 2017). The stress-strain formulation is versatile and can pronounce the benefits of high performance steel such as HYP400 steel compared to others. Figures 6c and 6d show illustrative examples of the simulated stress-strain relations of HYP400 and BCP325 steels under monotonic and cyclic loading histories. Referring to Figures 6c and 6d, the post-peak response of the equivalent stress-strain formulation is characterized by stress capping in compression; reloading in tension; cyclic deterioration in strength and stiffness; and local buckling stabilization. The difference between HYP400 and BCP325 steels is reflected in the enhanced yield and capping stress. In the post-capping region, the stress strain relations for both steels become similar due to local buckling stabilization.

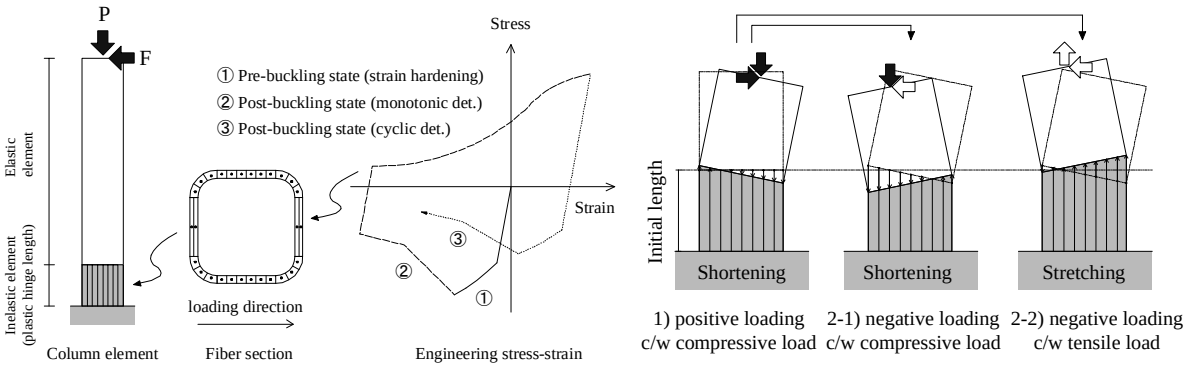

(a) modeling overview (b) schematic of axial shortening

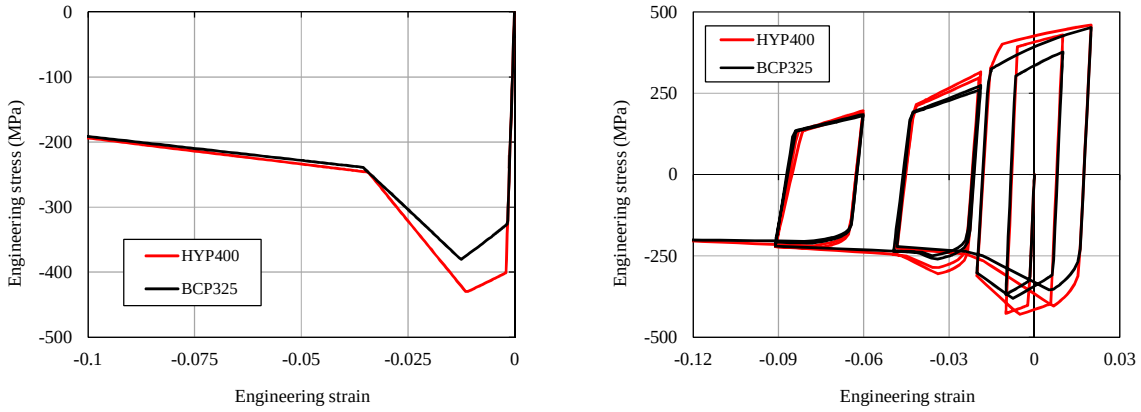

(c) monotonic load (d) cyclic load

Figure 6. Overview of fiber-based modeling approach and simulation comparisons of HYP400 and BCP325 steels

Figure 7 shows comparisons of the predicted steel beam-column response for the two steel types under consideration. The fiber-based model predicts well the collapse behavior of steel HSS columns.

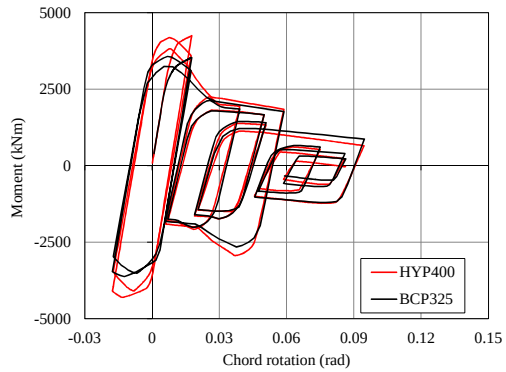

(a) moment-rotation, const. axial load

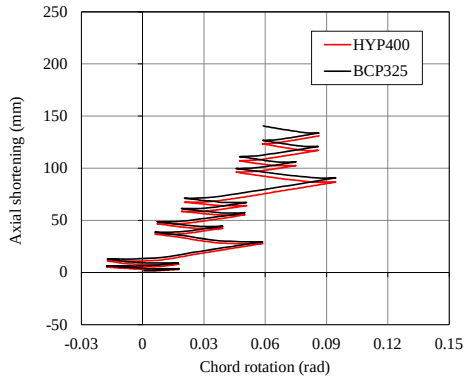

(b) axial shortening-rotation, const. axial load

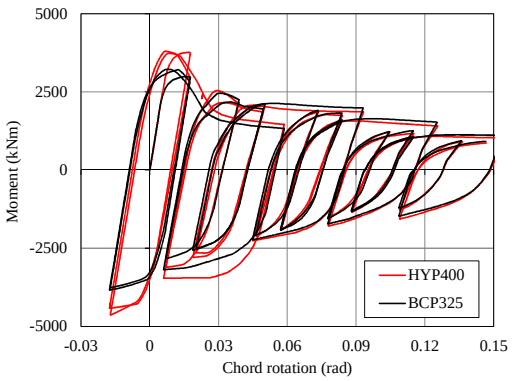

(c) moment-rotation, var. axial load

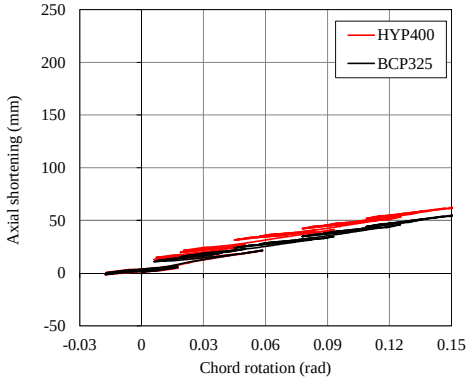

(d) axial shortening-rotation, var. axial load

Figure 7. Representative collapse simulations with the fiber-based deterioration model

5. PRELIMINARY COLLAPSE ASSESSMENT OF A STEEL MOMENT RESISTING FRAME

This section summarizes the collapse assessment of a steel MRF to demonstrate the potential use of HYP400 steel for improving a steel MRF's collapse capacity. For this purpose, a 2-dimensional 8-story steel MRF with HSS columns and wide flange steel beams is employed (see Figure 8). The design details of this steel MRF are summarized in Inoue et. al. (1995). The steel column D/t ratio is 27. In the original design, steel HSS columns in 1st to 6th stories were designed with BCP325 steel. A second case is considered herein in which the steel column material is replaced with HYP400 steel. The column section geometry is the same in both cases. The composite action effects are considered as discussed in Elkady and Lignos (2014). Figure 8b shows the SCWB ratio profile along the height of the steel MRF. It is computed based on the interior beam-to-column joints because this is where it is deemed to be critical. When the HYP400 steel material is utilized, the corresponding SCWB ratio is improved from 1.04 to 1.24 at the second-floor level. The steel MRF is modeled in the Open System for Earthquake Engineering Simulation (OpenSees) platform (McKenna 1997). Steel columns are modeled with the fiber-based deterioration model discussed in Section 4. Steel beams are modeled with the modified Ibarra-Medina-Krawinkler (IMK) model (Ibarra et. al. 2005, Lignos and Krawinkler 2011). The panel zone shear distortion is modeled with the Krawinkler trilinear model (Gupta and Krawinkler 1999). Viscous damping is approximated with the Rayleigh damping model. The assumed damping ratio is 2% at the first period, T_1 and at $0.25T_1$ of the corresponding steel MRF. The steel MRF is subjected to the N-S component of the JR Takatori record from the 1995 Kobe earthquake. To determine the collapse capacity of the steel MRFs, the JR Takatori record is scaled incrementally through collapse.

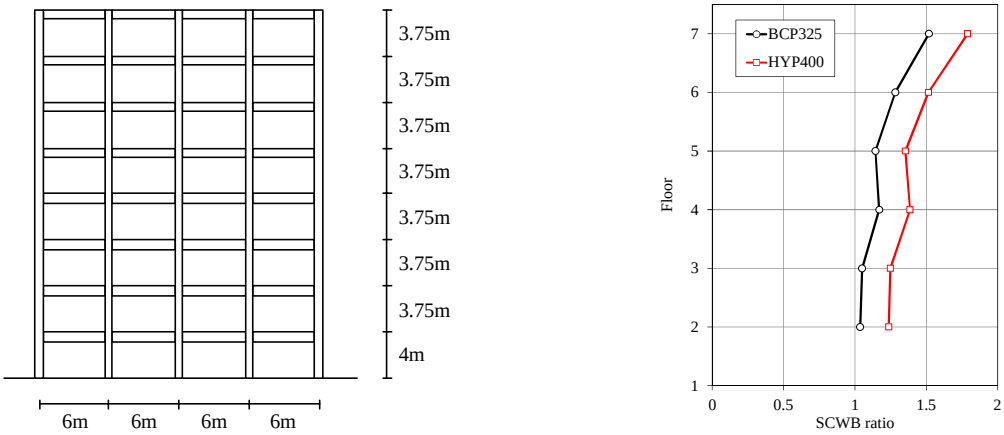

(a) elevation view (b) SCWB ratio at interior column

Figure 8. Analyzed 8-story steel MRF

Figures 9a and 9b show plots of the first mode spectral acceleration at the fundamental period of the steel MRF, $S_a(T_1)$, versus maximum and residual first story drift ratios (SDRs); the residual axial shortening of the first story columns is shown in Figure 9c. Referring to Figure 9a, the maximum SDR is reduced and the collapse capacity is slightly increased when the HYP400 steel is utilized. The biggest benefit of this material can be illustrated in Figure 9b that shows the $S_a(T_1)$-residual first SDR relation of the steel MRF. When a steel column utilizes HYP400 steel, the residual SDR remains within 0.005 radians up to $S_a(T_1)$=3.2g. This is because the HYP400 steel columns have a higher yield and capping moment (see Figure 5). Therefore, losses due to demolition may be considerably reduced (Ramirez and Miranda 2012). Referring to Figure 9c, although small in this case due to the ground motion nature (i.e. near-fault), the HYP400 steel material shows premise in reducing the column axial shortening due to local buckling.

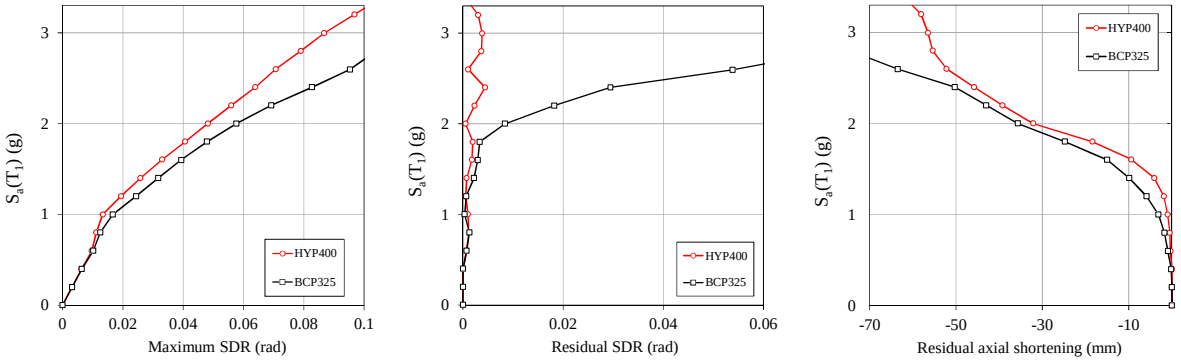

(a) maximum SDR of first story (b) residual SDR of first story (c) residual axial shortening of first story columns

Figure 9. Responses of 8-story steel MRF; global and local engineering demand parameters

Figure 10 shows responses of the first story center column when the ground motion is scaled $S_a(T_1)$=2.6g. Referring to Figure 10a, the moment-rotation of the column bottom end deteriorates in both cases once flexural yielding followed by local buckling occurs. Referring to Figure 10b, the HYP400 steel column remains almost elastic. On the other hand, the BCP325 steel column develops a plastic hinge at its top end. Therefore, a first story collapse mechanism (i.e. column hinging mechanism) forms when BCP325 steel columns are utilized. This is the main reason why the residual SDR increases for BCP325 steel columns (see Figure 9b). Referring to Figure 10c, the progression of axial shortening between the HYP400 and BCP325 steel columns is different. When the BCP325 steel column is utilized, both the column top and bottom deteriorate. Therefore the axial shortening of the BCP325 steel column is more than that of the HYP400 steel column.

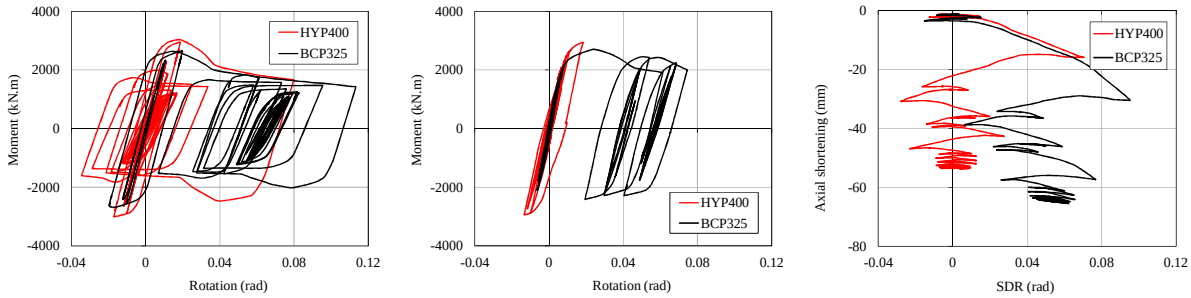

(a) moment-rotation of column bottom end

(b) moment-rotation of column top end

(c) axial shortening-SDR

Figure 10. First story interior column: Hysteretic behavior at $S_a(T_1)$=2.6g

6. SUMMARY

This paper presents a material-to-system level study that illustrates the potential of high performance steel materials for earthquake risk mitigation of steel frame buildings. High performance steel in this case refers to High Yield Point (HYP400) steel that is produced with TMCP technology through grain size refinement. The basic differences of the material stress-strain characteristics of such steels with other conventional steels are illustrated based on uniaxial monotonic and cyclic coupon tests. Component level virtual tests are conducted through detailed finite element analysis to demonstrate the differences in the pre- and post-peak response of steel beam-columns when the HYP400 steel is employed. The steel material potential is captured within a versatile fiber-based formulation that adequately reflects both the cyclic hardening and the post-buckling behavior of steel columns. Finally, collapse simulations of an 8-story steel MRF are carried out. The main findings of this study are summarized as follows:

- HYP400 steel is manufactured through TMCP technology that ensures 400MPa of nominal yield strength and a yield-to-tensile strength ratio of not more than 0.9.
- Standard uniaxial coupon test results suggest that HYP400 steel achieves higher yield strength but less strain hardening than conventional BCP325 steel. However, the ultimate strength of HYP400 steel is the same with BCP325 steel.
- Detailed finite element simulations suggest that HYP400 steel HSS columns reach a higher yield and capping moment compared to BCP325 steel columns of identical geometry. Although the post-capping behavior of the HYP400 and BCP325 steel columns is similar, the moment-rotation relation of the HYP400 steel column envelopes that of the BCP325 steel column.
- The axial shortening growth of the HYP400 and BCP325 steel columns with respect to the cumulative plastic rotation is the same regardless the employed loading history.
- A stress-strain formulation that captures the differences of various steel materials is developed and assigned to a fiber deterioration model. The proposed model is able to simulate reasonably well the moment-rotation and axial shortening of HYP400 and BCP325 steel columns subjected to cyclic loading.
- System level collapse simulations demonstrate that the use of HYP400 steel columns can potentially enhance the collapse capacity of steel MRFs and reduce potential residual deformations in the aftermath of earthquakes.

7. REFERENCES

ABAQUS (2014). ABAQUS/CAE User's Guide version 6.14. Dassault Systèmes Simulia Corp., Providence, RI.

Cornell CA, Krawinkler H (2000). Progress and Challenges in Seismic Performance Assessment. *PEER Center News*, 3, 1-3.

Elkady A, Lignos DG (2014). Modeling of the composite action in fully restrained beam-to-column connections: implications in the seismic design and collapse capacity of steel special moment frames. *Earthquake Engineering & Structural Dynamics*, 43, 1935‐1954.

Gupta A, Krawinkler H (1999). Prediction of seismic demands for SMRFs with ductile connections and elements. *SAC Background Report*, SAC/BD-99/06.

Ibarra LF, Medina RA, Krawinkler H (2005). Hysteretic models that incorporate strength and stiffness deterioration. *Earthquake Engineering & Structural Dynamics*, 34(12), 1489–1511.

Inoue K, Higashi K, Ogawa K, Tada M, Hasegawa T (1995). Earthquake response of structural members of rigid frames with RHS columns (Part 1-3). *Summaries of Technical Papers of Annual Meeting*, AIJ, Japan. (In Japanese)

Kawashima Y, Nishimura M (1973). Study on buckling strength of steel hollow square sections (Effect of welding and cold forming). *Summaries of Technical Papers of Annual Meeting*, AIJ, Japan. (In Japanese)

Krawinkler H, Zohrei M (1983). Cumulative damage in steel structures subjected to earthquake ground motions. *Computers & Structures*, 16(1–4), 531–541.

Lemaitre J, Chaboche JL (1975). A non-linear model of creep-fatigue damage cumulation and interaction (for hot metallic structures). *Mechanics of Visco-Elastic Media and Bodies*.

Lignos DG, Krawinkler H (2011). Deterioration modeling of steel components in support of collapse prediction of steel moment frames under earthquake loading. *Journal of Structural Engineering*, ASCE, 137 (1): 1291-1302.

Lignos DG, Suzuki Y (2013). Annual report of collapse assessment of steel moment resisting frames designed with high yield ratio steel columns, *Technical report at McGill University*, McGill University.

McKenna F (1997). Object-oriented finite element analysis: Frameworks for analysis, algorithms and parallel computing. *PhD dissertation*, University of California, Berkeley, CA.

Nishioka K, Ichikawa K (2012). Progress in thermomechanical control of steel plates and their commercialization. *Science and Technology of Advanced Materials*, 13, 1–20.

Ramirez CM, Miranda E (2012). Significance of residual drifts in building earthquake loss estimation. *Earthquake Engineering & Structural Dynamics*, 41:1477-1493.

Sousa AC, Lignos DG (2017). On the Inverse Problem of Classic Nonlinear Plasticity Models-An application to cyclically loaded structural steels. Report No. 231968, Resilient Steel Structures Laboratory (RESSLab), Ecole polytechnique Fédérale de Lausanne (EPFL).

Suzuki T, Suzuki Y, Yoshida Y, Kubota S, Shimura Y, Nagata M (2008). Development of structural steel for buildings with high yield ratio and high yield point leading innovative steel structural system. *Nippon Steel Technical Report*, No.97:64-73.

Suzuki Y, Lignos DG (2014). Development of loading protocols for experimental testing of steel columns subjected to combined high axial load and lateral drift demands near collapse. *10th National Conference on Earthquake Engineering*, EERI, Anchorage, Alaska.

Suzuki Y, Lignos DG (2015). Large scale collapse experiments of wide flange steel beam-columns. *8th International Conference on Behavior of Steel Structures in Seismic Areas (STESSA)*, Shanghai, China.

Suzuki Y, Lignos DG (2017). Collapse behavior of steel columns as part of steel frame buildings: experiments and numerical models. *16th World Conference on Earthquake (WCEE)*, Santiago Chile.

Yamada S, Akiyama H, Kuwamura H (1993). Post-buckling and deteriorating behavior of box-section steel members. *Journal of Structural and Construction Engineering*, AIJ, 444, 135–143. (in Japanese)

Wada A (2008). Damage controlled structures for strong earthquake. *High level seismic conference*, China.